




Effects of Nd_2O_3 substitution on the mechanical and radiation shielding properties of aluminoborobismuthate glasses

M. A. M. Uosif^{1,2}, A. M. A. Mostafa^{1,2}, Z. A. Alrowaili¹, Reda Elsaman²,
A. A. Showahy², Shams A. M. Issa^{2,3,a} , Yasser B. Saddeek^{2,4}

¹ Physics Department, College of Science, Jouf University, Al-Jouf, P.O. 2014, Sakaka, Saudi Arabia

² Physics Department, Faculty of Science, Al-Azher University, Assuit 71524, Egypt

³ Department of Physics, Faculty of Science, University of Tabuk, Tabuk, Saudi Arabia

⁴ Physics Department, College of Science in Zulfi, Majmaah University, Al Majma'ah 11952, Saudi Arabia

Received: 15 February 2021 / Accepted: 9 April 2021

© The Author(s), under exclusive licence to Società Italiana di Fisica and Springer-Verlag GmbH Germany, part of Springer Nature 2021

Abstract The current work is intended to examine the experimental mechanical, structural and photon shielding qualities of the $(58 - x)\text{B}_2\text{O}_3 - 30\text{Bi}_2\text{O}_3 - 10\text{Al}_2\text{O}_3 - 1\text{CoO} - x\text{Nd}_2\text{O}_3$ ($1 \leq x \leq 5$ mol%) glasses, labeled as Nd1, Nd2, Nd3, Nd4 and Nd5, which prepared via the melt quenching technique. The bulk density of the glasses was boosted with increasing Nd_2O_3 . XRD patterns were obtained to reveal the amorphous structure of the glasses. Mechanical parameters have been determined experimentally for all glasses. The elastic modulus values increase with increasing Nd_2O_3 content. To determine photon shielding parameters of all glasses, the mass attenuation coefficients (μ_m) were gained experimentally at 356 and 662 keV gamma-ray energies. Both shielding parameters of prepared glasses such as Half Value Layer ($T_{1/2}$) and Mean Free Path (λ) were reached using μ_m values. The lowest $T_{1/2}$ and λ values were observed in the Nd5 glass with the highest Nd_2O_3 contribution (5 mol%). It can be concluded that Nd_2O_3 addition to glass network improves mechanical properties and nuclear radiation security qualities.

1 Introduction

It is well known that various kinds of radiations such as gamma and X-ray emission are from the natural background radiation sources and man-made synthetic radiation sources such as medical equipment, nuclear reactors as well as nuclear weapons. Depending on the radiation type and its energy, possible harmful effects are also revealed with previous works. When it comes to natural radiation, special precautions can be taken. These precautions could be listed as defining the amount of natural radioactivity and designing of living spaces properly. However, the case may be totally different in artificial radiation sources and its facilities. It is highly wanted to save living tissues and environment from the ionizing radiation according to well-known ALARA principle. This protection proceedings especially perform by decreasing the radiation to the safe level by utilization of convenient shielding materials. Traditionally,

^a e-mail: shams_issa@yahoo.com (corresponding author)

concrete and lead are known as most used shielding materials due to their superior attenuation properties against gamma-ray and x-ray. Their employment could be performed not only in radiation staff equipment but also in shielding of radiation facilities as well as radioactive sources. In addition to mentioned shield kinds, different materials such as ceramics, polymers, concrete and alloys have been proposed as radiation shielding materials in previous studies [1–3]. Among the alternative shielding materials, glasses are utilized as radiation protection substances instead of traditional materials [4]. This is because glasses are reputed by high-level optical clarity and can be produced in varied sizes and shapes.

The literary analysis reveals the various drawbacks of lead (Pb) and plumbing products such as toxicity, nontransparency and inadequate longevity. Therefore, importance of creation and use of alternative and eco-friendly radiation shields has become obvious in the literature. U. Perişanoğlu et al. studied the structural, gamma-ray, and neutron radiation protection characteristics of $(50 - x)\text{B}_2\text{O}_3:40\text{PbO}:10\text{Li}_2\text{O}:x\text{Ag}_2\text{O}$ glass system. They found that the addition of Ag_2O content increases the radiation shielding parameters [5]. A.S. Abouhaswa et al. examined nuclear radiation shielding properties of a novel glass system, which has nominal compositions $(40 - x)\text{B}_2\text{O}_3:40\text{Pb}_3\text{O}_4:20\text{ZnO}:x\text{Er}_2\text{O}_3$. They reported that the increasing Er_2O_3 additive upgraded the prepared glasses in the attenuation of neutrons as in gamma rays. In addition, the protection ability of the fabricated glasses against alpha and proton charged particles was also evaluated [6].

A.S. Abouhaswa and Esra Kavaz investigated the impacts of HgO addition on optical, structural and radiation shielding properties of newly developed BNBH glass system, with nominal composition $(60 - x)\text{B}_2\text{O}_3:20\text{Na}_2\text{O}:20\text{BaO}:x\text{HgO}$. They perceived that the insertion of HgO improved the protecting competences of the glasses against several nuclear radiation types [7]. Esra Kavaz et al. fabricated and examined the strontium vanadate glasses with the nominal composition $(\text{V}_2\text{O}_5)_{60}:(\text{SrO})_{(40-x)}:(\text{PbO})_x$ for optical, structural, physical and nuclear radiation shielding qualities. They found that with PbO added content instead of SrO , the Z_{eq} values increased while HVL, EBF and EABF values reduced. In addition, since the addition of PbO enhanced the density, the capacity of VSP glasses to retain fast neutrons was also increased [8]. G. Sathiyapriya et al. studied structural, optical and nuclear radiation shielding properties of strontium barium borate glasses doped with dysprosium and niobium [9].

In the updated times, the area of studying borobismuthate glasses doped with rare earth oxides (REO) had been expanded due to their wide-ranging imaginable potentials in many scientific fields. Such fields comprise optical devices, radiation shielding, etc. [10–16]. The noteworthy features of REO are based in altering the physical and chemical environment of the phonon energies the host glasses. These features are due to the large number of energy levels of and 4f–4f transitions REO. On the other hand, Nd_2O_3 is one from REO and is the utmost effective applicants for multipurpose. These purposes are ranging from the use in halogen lamps as an ultraviolet absorbent and the utilization in giving high rigidity and chemical durability in refractory glasses to the effective glass shielding and laser-based glasses [17–19].

The mixture of Bi_2O_3 and B_2O_3 permits alteration of the physical properties of borobismuthate glasses in a wide range depending on the composition. Comparing with different glass hosts, the physical properties of the environment of borobismuthate glasses have drawn more attention. These properties are concentrated in their high densities and high refractive indices. The borobismuthate glasses usually had multiconcentrations of $[\text{BO}_3]$, $[\text{BO}_4]$, $[\text{BiO}_3]$, or $[\text{BiO}_6]$ structural units. Increase or decrease in the former structural units depends on the concentration of Bi_2O_3 and the concentration of other dopants such as Nd_2O_3 [20, 21]. According to the preceding arguments, in the current study the host content of the glass

Table 1 Chemical composition and density of the prepared glasses

Sample code	mol%					wt%					ρ (g/cm ³)	
	Nd ₂ O ₃	B ₂ O ₃	Bi ₂ O ₃	Al ₂ O ₃	CoO	Nd	O	B	Bi	Al		Co
Nd1	1	58	30	10	1	0.008574	0.481408	0.180131	0.269097	0.052925	0.007865	5.735
Nd2	2	57	30	10	1	0.017147	0.475941	0.177025	0.269097	0.052925	0.007865	5.907
Nd3	3	56	30	10	1	0.025721	0.470473	0.173920	0.269097	0.052925	0.007865	5.962
Nd4	4	55	30	10	1	0.034294	0.465005	0.170814	0.269097	0.052925	0.007865	6.000
Nd5	5	54	30	10	1	0.042868	0.459537	0.167708	0.269097	0.052925	0.007865	6.176

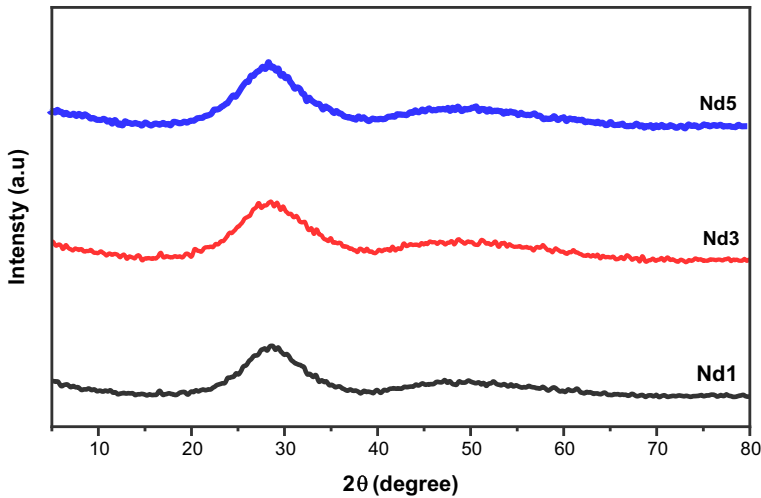


Fig. 1 XRD patterns of the prepared glasses system

system $(58 - x)\text{B}_2\text{O}_3 - 30\text{Bi}_2\text{O}_3 - 10\text{Al}_2\text{O}_3 - 1\text{CoO} - x\text{Nd}_2\text{O}_3$ is doped with different concentrations of Nd_2O_3 ($1 \leq x \leq 5$ mol%). The mechanical and radiation shielding parameters of this glass matrix will be explored.

2 Experimental section

The multiple components of bismuth aluminoborate with nominal chemical composition of $(58 - x)\text{B}_2\text{O}_3 - 30\text{Bi}_2\text{O}_3 - 10\text{Al}_2\text{O}_3 - 1\text{CoO} - x\text{Nd}_2\text{O}_3$ ($1 \leq x \leq 5$) were fabricated by regular melt-quenching technique. Table 1 shows these compositions. The purity of chemical powder (99% purity grade) of H_3BO_3 , Bi_2O_3 , Al_2O_3 , CoO and Nd_2O_3 was employed for glass preparation. The powder mix was preheated into ceramic crucible at 400°C for 1 h to eliminate H_2O . The mix was then heated to melting process at 1050°C at 1 h. The molten was cast into cylindrical brass mold and then heated for annealing at 400°C for 1 h.

The type of amorphous arrangement of the prepared glasses is deduced from the obtained XRD diffraction patterns. X-ray diffraction analysis was performed in the range $4^\circ - 70^\circ$ in 2θ -scale by using Philips PW/1710 with $\text{Cu-K}\alpha$ radiation source. Figure 1 shows as-prepared XRD for all studied samples, respectively. These figures demonstrated that all studied samples did not show any sharp peaks and only one broad hump around 28° can be detectable. The absorption FTIR of the prepared glasses was managed via KBr tool in the range $400 - 2000\text{ cm}^{-1}$ and by using JASCO, FT/IR-430 (Japan). The density of the prepared glasses was detected by using conventional Archimedes technique with acetone as the immersion liquid. The pulse-echo technique is used to measure the longitudinal and shear ultrasonic velocities. The velocities besides the density can be used to determine the elastic properties of the prepared glasses. The accuracy for the two velocities is ± 10 m/s.

Gamma spectroscopy system shown in Fig. 2 is used to measure the linear attenuation coefficient (μ) of the fabricated glasses. Using 356 and 662 keV gamma emitted from ^{133}Ba ($1\ \mu\text{Ci}$) and ^{137}Cs ($5\ \mu\text{Ci}$) sources, the gamma-ray shielding parameters were measured. The Al window thickness in this detector is 0.5 mm and has a resolution of 7.5% at 0.662 meV

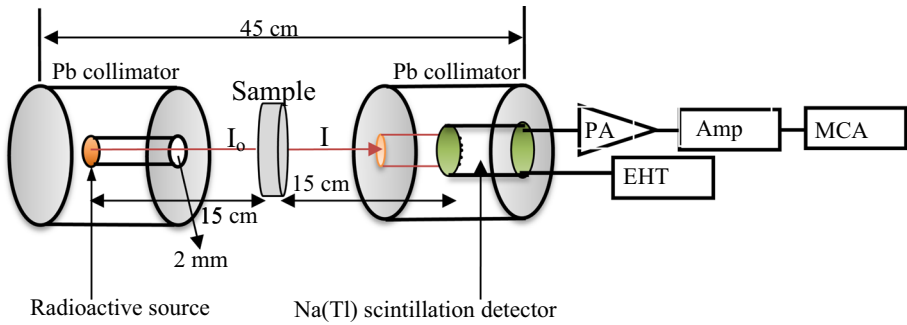


Fig. 2 Experimental setup of gamma shielding measurements

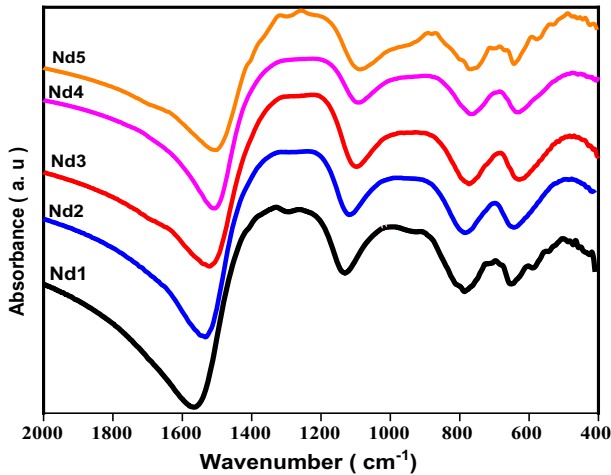


Fig. 3 FTIR spectra of the prepared glasses system

energy emitted from ^{137}Cs . All samples were measured for about 4 h, and this measurement repeated three times.

3 Results and discussion

3.1 Analysis of FTIR results

The FTIR spectroscopy tests as shown in Fig. 3 were utilized to study the effect of Nd_2O_3 on the organizations of the structural units of borobismuthate network. According to the mentioned figure, the active bands of the studied network are two narrow bands around 488 and 698 cm^{-1} and two broader bands at around 888–1025 and 1215–1350 cm^{-1} . Increment of Nd_2O_3 shifted the bands to higher frequencies, and the bands at around 888–1025 and 1215–1350 cm^{-1} will be wider. The detected wider bands are superposition of some specific bands. Separation of this superposition of bands required a deconvolution process in Gaussian bands to specify the center (Cen) and the relative area (Ar) of each specific band. Ar can be attributed to the concentration of a specific structural unit. The values of the parameters Cen

Table 2 Deconvolution parameters of the FTIR of $(58 - x)\text{B}_2\text{O}_3 - 30\text{Bi}_2\text{O}_3 - 10\text{Al}_2\text{O}_3 - 1\text{CoO} - x\text{Nd}_2\text{O}_3$ glasses and their assignments. C is the center of the band and A is the relative area (%) of the band

Nd1	Nd2		Nd3		Nd4		Nd5		Assignment
	A	C	A	C	A	C	A	C	
2.69	494	466	2.85	497	2.34	494	3.97	500	Bi–O–Bi in BiO6 octahedral [15, 16]
2.48	550	536	3.02	535	1.96	543	3.80	556	AlO6 structural units [17, 18]
4.57	716	707	5.51	715	4.20	718	5.45	710	bending of B–O–B in BO3 triangles [19, 20]
11.93	893	888	12.74	895	12.63	888	3.93	838	The B–O stretching vibration in BO4 units [21]
–	–	–	–	–	–	–	10.14	904	
11.53	998	1039	15.47	1024	15.79	1018	13.36	1025	BO4 tetrahedra [22, 23]
8.79	1082	–	–	–	–	–	–	–	
11.40	1186	1200	21.04	1193	16.87	1167	15.82	1176	
13.50	1261	1300	19.40	1299	17.01	1260	16.42	1259	B–O asymmetric stretching vibrations in BO3 unit [24–26]
18.05	1349	1389	13.07	1375	17.69	1347	16.59	1339	
15.06	1442	1454	6.90	1436	11.51	1426	10.55	1416	stretching vibrations of the B–O of trigonal BO3 units [27, 28]
0.45	–	–	0.46	–	0.47	–	0.48	–	N4

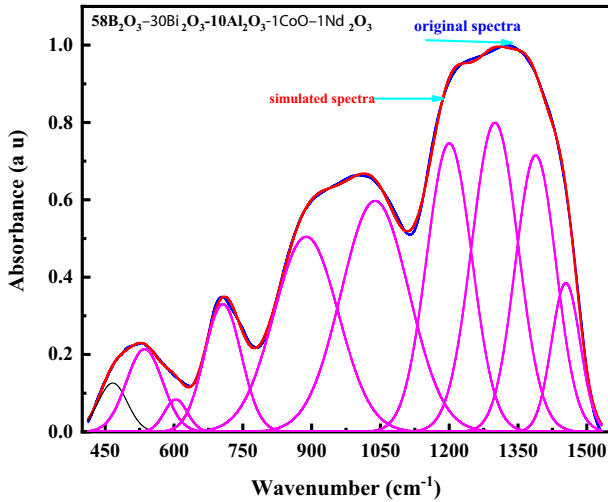


Fig. 4 Curve fitting of FTIR spectra of the glasses $58\text{B}_2\text{O}_3\text{-}30\text{Bi}_2\text{O}_3\text{-}10\text{Al}_2\text{O}_3\text{-}1\text{CoO-}1\text{Nd}_2\text{O}_3$

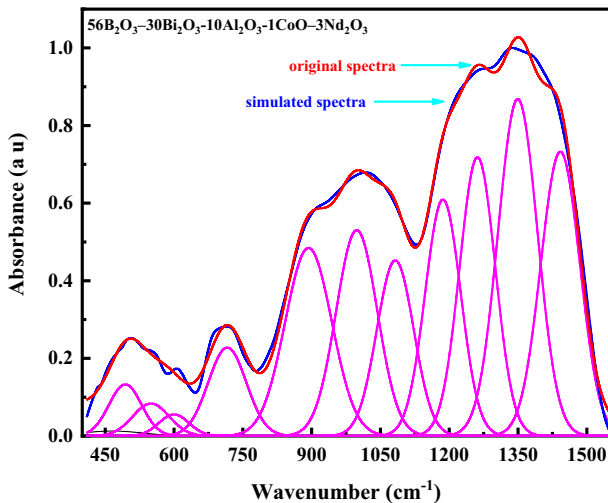


Fig. 5 Curve fitting of FTIR spectra of the glasses $56\text{B}_2\text{O}_3\text{-}30\text{Bi}_2\text{O}_3\text{-}10\text{Al}_2\text{O}_3\text{-}1\text{CoO-}3\text{Nd}_2\text{O}_3$

and Ar for each Nd_2O_3 concentration are given in Table 2 with their assignments [22–31]. Moreover, from the deconvolution process, the fraction N4 of 4-coordinated boron's in each glass sample can be determined. Figures 4, 5 and 6 depict the spectrum deconvolution of three glass samples. The samples had 1 Nd_2O_3 , 3 Nd_2O_3 and 5 Nd_2O_3 in mol%, respectively.

It is evident from Table 2 the increment of N4 as a function of Nd_2O_3 content. This is agreeing with the broadening of the $888\text{--}1025$ and $1215\text{--}1350\text{ cm}^{-1}$ bands and their shift to higher frequencies and the constancy of the vibrations related to BiO_6 or AlO_6 structural units [23]. The mentioned shift is associated with the creation of B–O–Nd bonds. The increment of N4 can be attributed to the converted nonbridging oxygens associated with BO_3 into bridging oxygens associated with BO_4 structural units. This procedure can be performed

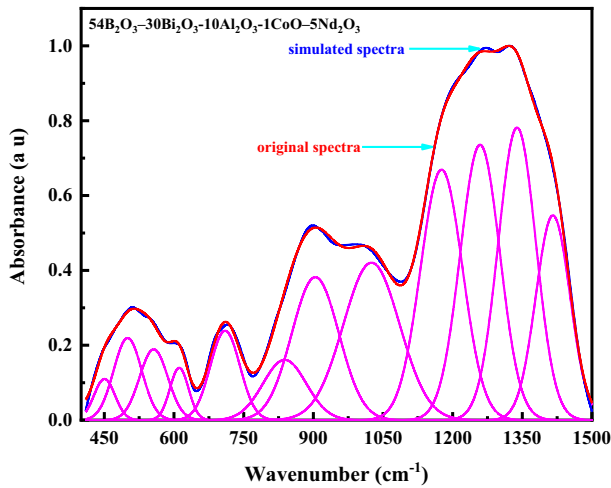


Fig. 6 Curve fitting of FTIR spectra of the glasses $54\text{B}_2\text{O}_3-30\text{Bi}_2\text{O}_3-10\text{Al}_2\text{O}_3-1\text{CoO}-5\text{Nd}_2\text{O}_3$

by breaking trigonal BO_3 and increasing the coordination number as Nd_2O_3 had NdO_7 structural units. This proposes that Nd_2O_3 changes the borobismuthate links by strengthening and polymerizing the network of the explored glasses and presents acceptable chemical surroundings for Nd^{3+} for its moderate incorporation equivalently into the glasses. This means that the addition of Nd_2O_3 to borobismuthate network will increase its compactness and rigidity [32].

3.2 Analysis of the mechanical properties

Table 3 lists the values of the mechanical properties. The listed mechanical properties are the two ultrasonic velocities, longitudinal and shear elastic moduli along with the bulk modulus and Young's modulus. The increment of the density as a function of Nd_2O_3 as tabulated in Table 1 point to that the increment of Nd_2O_3 causes an increase in the density. Such an increment can be attributed to the difference in the relative molar mass of the B_2O_3 and Nd_2O_3 . The relative molar mass of the B_2O_3 and Nd_2O_3 is 69.9 and 336.5, respectively. Similarly, the increment of the density points to that Nd_2O_3 compacts the network of the explored glasses by the increment of the number of bridging oxygens [33]. As depicted in Fig. 4, the increment of the two ultrasonic velocities as a function of Nd_2O_3 is ascribed to the creation of strengthen $\text{B}-\text{O}-\text{Nd}$ bonds that replaced low-strength $\text{B}-\text{O}-\text{Bi}$ chemical bonds. Moreover, the shift of the FTIR bands to increased wave number associated with the creation of bridging oxygens causes an increase in the rigidity of the borobismuthate glass network. Furthermore, the Nd^{3+} ions may replace Bi^{3+} in the explored network. This replacement can be ascribed to the slight difference in Pauling ionic radii between Nd^{3+} and Bi^{3+} . Thus, the network will be compacted and its rigidity will increase. This argument accounts for the increment of the two ultrasonic velocities [34]. Figure 5 depicts the increment of the mechanical properties as a function of Nd_2O_3 . The increment of the mechanical properties can be ascribed to the increment in the coordination number, the cross-link density and the number of bonds of the network. Another reason for the increment of the mechanical properties is the retraction of the surroundings around Nd^{3+} due to the enhanced field strength of Nd^{3+} ions.

Table 3 Longitudinal velocity (V_L), shear velocity (V_S), longitudinal modulus (L), shear modulus (G), bulk modulus (K) and Young's modulus of the prepared glasses

Sample code	V_L (m/s)	V_S (m/s)	L (GPa)	G (GPa)	K (GPa)	Y (GPa)
Nd1	4350	1950	109	22	79	60
Nd2	4560	2170	122	28	85	75
Nd3	4710	2232	132	30	93	81
Nd4	4760	2300	137	32	94	86
Nd5	4950	2460	151	37	102	100

3.3 Gamma shielding properties

In this study, five different borobismuthate glasses were investigated in terms of their radiation attenuation capabilities. Figure 2 displays the setup used to experimental test of gamma-ray transmission in a laboratory. From Fig. 2, it can be shown that studied sample was between radioactive source and NaI (Tl) scintillation detector. This is a standard method of study in the field of gamma-ray transmission studies. To boost the functionality of NaI (Tl) scintillation detector, Pb collimators were also used. Its primary objective is to quantify the number of photons which pass through the specimens of prepared waste samples as candidate attenuator materials for ionizing radiation facilities. Mass attenuation coefficients (μ_m) of five samples encoded Nd1, Nd2, Nd3, Nd4 and Nd5 were found at 356 and 662 keV, respectively. The experimental work was validated using the XCOM program. The data used to find μ_m for radioisotope energies are 356 and 662 keV. μ_m agreed well with XCOM program (Table 4).

Figure 7 shows the variation of experimental μ_m values versus glass composition for samples. It can be seen from the figure that μ_m values decrease with increment in photon energy. As the Nd_2O_3 content increases from 1 to 5% (mol) in the glass samples, the material densities increase from 5.735 to 6.176 g/cm^3 (see Table 1). 0.15185, 0.15238, 0.15295, 0.15378, and 0.15441 (cm^2/g) are the experimental mass attenuation coefficient (μ_m) values at 356 keV for Nd1, Nd2, Nd3, Nd4, and Nd5 glass samples, respectively. However, the highest μ_m values were reported for Nd5 sample, which has the highest Nd_2O_3 content in the chemical structure (see Table 1). This is a confirmation of the synergistic effect of increasing Nd_2O_3 content on gamma-ray attenuation properties. Figure 8 indicates the patterns of the half value layer ($T_{1/2}$) values for the five test samples of the present research. In Fig. 8, it can be seen that the lowest $T_{1/2}$ values were reported for 356 keV, whereas the highest $T_{1/2}$ values for 662 keV. This can be explained by the penetration abilities of gamma rays depending on their energy. In other words, lowest gamma-ray energy requires the minimum material thickness to be stopped. Moreover, it can be seen that Nd5 sample showed the minimum $T_{1/2}$ values among the investigated samples. This is also another confirmation of superior shielding property of Nd5 sample among the fabricated waste specimens. Figure 9 presents the variation of experimental mean free path (λ) values with photon energy for the waste samples. Similar to variation trend in $T_{1/2}$ values, the lowest λ values were reported for Nd5 sample. Effective atomic number (Z_{eff}) and effective electron density (N_{el}) values are listed in Table 5. As presented in this table, Z_{eff} and N_{el} values increase as the Nd_2O_3 content increases. 26.90, 27.00, 27.10, 27.24, and 27.35 are the effective atomic number (Z_{eff}) values at 356 keV for Nd1, Nd2, Nd3, Nd4, and Nd5 glass samples, respectively. The Nd5 glass sample has the highest Z_{eff} and N_{el} values.

Table 4 Experimental (Exp.) and theoretical (XCOM) mass attenuation coefficients (μ_m) (cm^2/g) of the prepared glasses

E (keV)	Nd1		Nd2		Nd3		Nd4		Nd5	
	Exp	XCOM Δ	Exp	XCOM Δ	Exp	XCOM Δ	Exp	XCOM Δ	Exp	XCOM Δ
356	0.15185	0.15190 0.03	0.15238	0.15250 0.08	0.15295	0.15310 0.10	0.15378	0.15370 0.05	0.15441	0.15430 0.07
662	0.08549	0.08557 0.09	0.08556	0.08564 0.09	0.08563	0.08570 0.08	0.08567	0.08577 0.11	0.08575	0.08584 0.11

Table 5 Effective atomic number (Z_{eff}) and effective electron density (N_{el}) of the prepared glasses

E (keV)	Nd1		Nd2		Nd3		Nd4		Nd5	
	Exp	Theo	Exp	Theo	Exp	Theo	Exp	Theo	Exp	Theo
Effective atomic number (Z_{eff})										
356	26.90	26.92	27.00	27.02	27.10	27.13	27.24	27.23	27.35	27.34
662	23.88	23.90	23.90	23.92	23.92	23.93	23.93	23.95	23.95	23.97
Effective electron density ($N_{\text{el}} \times 10^{23}$ (electron/g))										
356	3.40	3.40	3.41	3.41	3.42	3.42	3.44	3.44	3.45	3.45
662	3.01	3.02	3.02	3.02	3.02	3.02	3.02	3.02	3.02	3.03

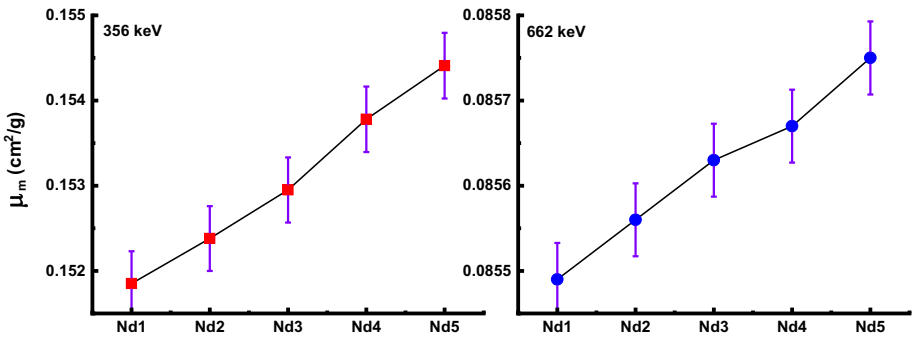


Fig. 7 Mass attenu

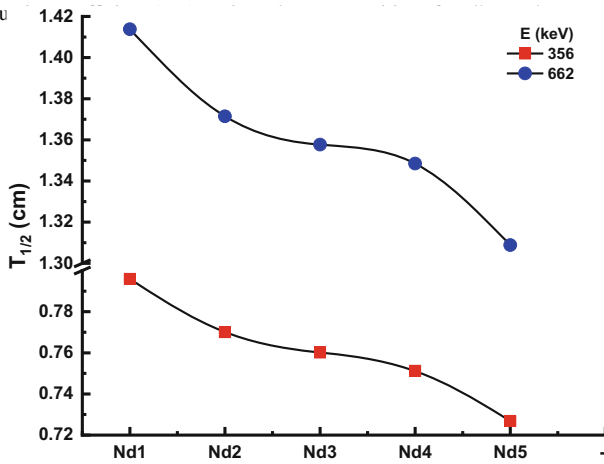


Fig. 8 Half value l

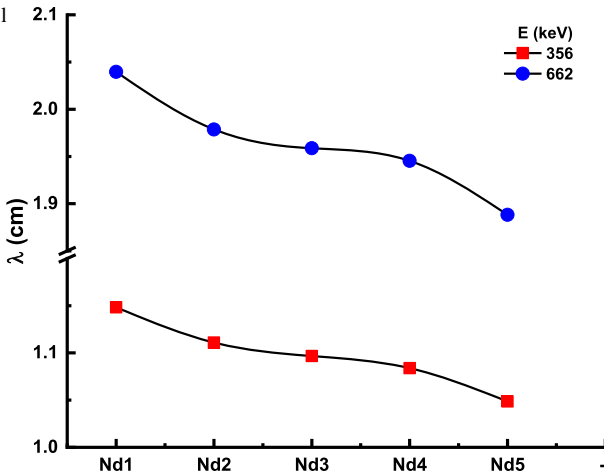


Fig. 9 Mean free path (λ) against glass compositions for all samples

4 Conclusion

This study was conducted to investigate whether the increasing Nd₂O₃ additive owns a positive impact on the structural, mechanical and nuclear protection characteristics of borobismuthate glasses. The density of all glasses showed an increasing behavior (from 5.735 to

6.176 g/cm³). XRD patterns of all glasses exhibited no crystalline peaks. Nuclear radiation safety capability of all glasses for photons neutrons was also extensively assessed at 356 and 662 keV. The μ_m values of all glasses experimentally measured: 0.15185, 0.15238, 0.15295, 0.15378, and 0.15441 (cm²/g), are the experimental mass attenuation coefficient (μ_m) values at 356 keV for Nd1, Nd2, Nd3, Nd4, and Nd5 glass samples, respectively, while the 0.08549, 0.08556, 0.08563, 0.08567 and 0.08575 (cm²/g) are the experimental mass attenuation coefficient (μ_m) values at 662 keV for Nd1, Nd2, Nd3, Nd4 and Nd5 glass samples, respectively. The biggest μ_m values ranged between 0.15441 and 0.08575 cm²/g and were achieved for the Nd5 glass. It is deduced from these results that Nd5 glass with high Nd₂O₃ concentration can be worthy of nuclear protection applications due to its good shielding, mechanical and structural features.

Acknowledgements The authors extend their appreciation to the Deanship Scientific Research at Jouf University KSA for funding the work through research Grant No. DSR 2020-04-503.

References

1. H.M.H. Zakaly, H.A. Saudi, S.A.M. Issa, M. Rashad, A.I. Elazaka, H.O. Tekin, Y.B. Saddeek, *Ceram. Int.* **47**, 5587–5596 (2020)
2. S.A.M. Issa, M. Ahmad, H.O. Tekin, Y.B. Saddeek, M.I. Sayyed, *Results Phys.* **13**, 102165 (2019)
3. S.A.M. Issa, H.A. Saudi, H.M.H. Zakaly, M. Rashad, A.I. Elazaka, M. Pyshkina, H.O. Tekin, *Ceram. Int.* **47**, 185–204 (2020)
4. E. Kavaz, *Radiat. Phys. Chem.* **160**, 112 (2019)
5. U. Perişanoğlu, H.O. Tekin, A.S. Abouhaswa, E. Kavaz, *Radiat. Phys. Chem.* **179**, 109262 (2021)
6. A.S. Abouhaswa, U. Perişanoğlu, H.O. Tekin, E. Kavaz, A.M.A. Henaish, *Ceram. Int.* **46**, 27849 (2020)
7. A.S. Abouhaswa, E. Kavaz, *Ceram. Int.* **46**, 16166 (2020)
8. E. Kavaz, E.H. Ghanim, A.S. Abouhaswa, *J. Non-Cryst. Solids* **538**, 120045 (2020)
9. G. Sathiyapriya, K.A. Naseer, K. Marimuthu, E. Kavaz, A. Alalawi, M.S. Al-Buriah, *J. Mater. Sci. Mater. Electron.* **32**, 8570 (2021)
10. I. Kashif, A. Abd El-Maboud, A. Ratep, *Results Phys.* **4**, 1 (2014)
11. K. Boonin, J. Kaewkhao, T. Ratana, P. Limsuwan, *Procedia Eng.* **8**, 207 (2011)
12. M. Djamal, L. Yuliantini, R. Hidayat, N. Rauf, M. Horprathum, R. Rajaramakrishna, K. Boonin, P. Yasaka, J. Kaewkhao, V. Venkatramu, S. Kothan, *Opt. Mater. (Amst.)* **107**, 110018 (2020)
13. G. Lakshminarayana, R. Vidya Sagar, S. Buddhudu, *J. Lumin.* **128**, 690 (2008)
14. Y.Q. Qiu, J. Kang, C.X. Li, X.Y. Dong, C.-L. Zhao, *Laser Phys.* **20**, 487 (2010)
15. W.M. Abd-Allah, A.M. Fayad, H.A. Saudi, *Opt. Quantum Electron.* **51**, 165 (2019)
16. M.A. Marzouk, H.A. ElBatal, A.M. Abdelghany, *SILICON* **10**, 29 (2018)
17. K. Boonin, J. Kaewkhao, N. Nuntawong, P. Limsuwan, *Procedia Eng.* **32**, 827 (2012)
18. J.T. James, J.K. Jose, M. Manjunatha, K. Suresh, A. Madhu, *Ceram. Int.* **46**, 27099 (2020)
19. K. Vijaya Kumar, A. Suresh Kumar, *Opt. Mater. (Amst.)* **35**, 12 (2012)
20. T. Honma, Y. Benino, T. Fujiwara, R. Sato, T. Komatsu, *Opt. Mater. (Amst.)* **20**, 27 (2002)
21. R. Ihara, T. Honma, Y. Benino, T. Fujiwara, T. Komatsu, *Opt. Mater. (Amst.)* **27**, 403 (2004)
22. Y.B. Saddeek, M.A. Kaid, M.R. Ebeid, *J. Non-Cryst. Solids* **387**, 30 (2014)
23. T. Satyanarayana, T. Kalpana, V. Ravi Kumar, N. Veeraiah, *J. Lumin.* **130**, 498 (2010)
24. M. Pal, K. Hirota, Y. Tsujigami, H. Sakata, *J. Phys. D: Appl. Phys.* **34**, 459 (2001)
25. R. Iordanova, Y. Dimitriev, V. Dimitrov, S. Kassabov, D. Klissurski, *J. Non-Cryst. Solids* **231**, 227 (1998)
26. A. Kumar, S.B. Rai, D.K. Rai, *Mater. Res. Bull.* **38**, 333 (2003)
27. Y. Cheng, H. Xiao, W. Guo, *Ceram. Int.* **34**, 1335 (2008)
28. Y. Cheng, H. Xiao, W. Guo, W. Guo, *Ceram. Int.* **33**, 1341 (2007)
29. P. Pascuta, L. Pop, S. Rada, M. Bosca, E. Culea, *J. Mater. Sci. Mater. Electron.* **19**, 424 (2008)
30. Y.B. Saddeek, M.S. Gaafar, *Mater. Chem. Phys.* **115**, 280 (2009)
31. K. El-Egili, *Phys. B Condens. Matter* **325**, 340 (2003)

32. Y.B. Saddeek, A.A. El-Maaref, K.A. Aly, M.M. ElOkr, A.A. Showahy, J. Alloys Compd. **694**, 325 (2017)
33. Y.C. Ratnakaram, N.V. Srihari, A.V. Kumar, D.T. Naidu, R.P.S. Chakradhar, Spectrochim. Acta Part A Mol. Biomol. Spectrosc. **72**, 171 (2009)
34. G.V. Rao, N. Vijaya, A.S. Joshi, H.D. Shashikala, C.K. Jayasankar CK, Soc. Glass Technol. **56**, 81 (2015)